Monoenergetic Ion Beam Generation by Driving Ion Solitary Waves with Circularly Polarized Laser Light

D. Jung,[1,2,3,*] L. Yin,[1] B. J. Albright,[1] D. C. Gautier,[1] R. Hörlein,[2,3] D. Kiefer,[2,3] A. Henig,[2,3] R. Johnson,[1] S. Letzring,[1] S. Palaniyappan,[1] R. Shah,[1] T. Shimada,[1] X. Q. Yan,[3] K. J. Bowers,[1] T. Tajima,[2] J. C. Fernández,[1] D. Habs,[2,3] and B. M. Hegelich[1,2]

[1]*Los Alamos National Laboratory, Los Alamos, New Mexico 87545, USA*
[2]*Department für Physik, Ludwig-Maximilians-Universität München, D-85748 Garching, Germany*
[3]*Max-Planck-Institut für Quantenoptik, D-85748 Garching, Germany*

(Received 21 March 2011; published 8 September 2011)

Experimental data from the Trident Laser facility is presented showing quasimonoenergetic carbon ions from nm-scaled foil targets with an energy spread of as low as ±15% at 35 MeV. These results and high-resolution kinetic simulations show laser acceleration of quasimonoenergetic ion beams by the generation of ion solitons with circularly polarized laser pulses (500 fs, $\lambda = 1054$ nm). The conversion efficiency into monoenergetic ions is increased by an order of magnitude compared with previous experimental results, representing an important step towards applications such as ion fast ignition.

DOI: 10.1103/PhysRevLett.107.115002 PACS numbers: 52.38.Kd, 41.75.Jv, 52.50.Jm, 52.65.Rr

Laser-ion acceleration has been of particular interest over the last decade for fundamental as well as applied sciences [1–3]. Remarkable progress has been made in producing laser-driven proton and ion accelerators [4–6] that are very compact compared with conventional RF accelerators. These beams have been produced with particle energies of several MeV per nucleon and outstanding properties in terms of transverse emittance and current, but they typically exhibit an exponential energy distribution. Almost all prospective applications for these ion beams, including oncology [7], proton imaging [8] and inertial confinement fusion [9,10], require quasimonoenergetic beams with a low energy spread. Up to now, the majority of high intensity laser experiments aiming for ion-acceleration have used comparatively thick targets in the μm range. In these target normal sheath acceleration (TNSA) experiments [11–13], hot thermal electrons are generated normal to the front and rear surfaces of the solid target that accelerate protons over a very short distance to energies of up to 67 MeV [2,14]. Here, the accelerated ions usually exhibit broad exponential energy spectra; by using *in situ* engineered targets, quasimonoenergetic spectra can be generated, but with low ion flux [15,16]. Recently, ion acceleration by radiation pressure acceleration (RPA) [17–20] has drawn a lot of attention. Here, the light pressure of a linearly polarized (LP) fs-laser pulse exceeding 10^{23} W/cm^2 drives an overcritical ($n_e/\gamma^e n_{\mathrm{cr}} > 1$, the relativistically corrected ratio of the electron to the critical electron density) nm-scaled target in the laser piston regime [21]; at lower intensity RPA can occur with circularly polarized (CP) laser. Simulations have shown that for a single species target, the laser can drive the plasma as a single block to a monoenergetic ion spectrum; in a multi-species target, lighter ions with higher charge to mass ratio ''snowplow'' ahead of the heavier species [22,23]. Experimental evidence of RPA has proven to be difficult; first experimental data indicating signatures of RPA has been reported by Henig *et al.* [24]; however, monoenergetic ion spectra have not been generated.

Here we report on the experimental generation of quasimonoenergetic carbon ion beams by driving ion solitons with CP laser pulses of 500 fs length and exceptionally high laser contrast in the relativistically transparent matter regime. First indications suggest that the ion energies and particle fluxes scale favorably with laser intensity. High-resolution 2D-VPIC [25] simulations matching the experiment's laser and target parameters reproduce the experimental data. In the simulations we observe the generation of an ion soliton and its propagation within the target and facilitating the ion acceleration. The experiments conducted at the Trident Laser facility [26,27] yielded quasimonoenergetic carbon ions with energies of 35 MeV and an energy spread as low as ±15%, in good agreement with the simulations. This proof-of-principle experiment demonstrates that laser-based particle sources are now capable of delivering the necessary ion energies for ion injectors and medical applications such as hadron therapy of skin or eye tumors.

In particular, we employ ultrathin nm-scaled foil targets, in contrast to [2,15], and combine these with CP laser pulses and ultrahigh contrast (OPAPE technique [27]) to reduce premature ionization and expansion of the target prior to the arrival of the pulse peak. Still, the long pulse duration of 500 fs (FWHM) and its shoulders of $\sim 10^{-5}$@5 ps (i.e., $>10^{15}$ W/cm^2) lead to preexpansion and a qualitative difference in the interaction compared with pure RPA acceleration as seen in PIC simulations (e.g., Klimo *et al.* [17]): the combination of a longer laser pulse and increased $\vec{j} \times \vec{B}$ heating of the electrons in the plasma will lead to relativistic transparency of the target

[28] ($n_e/\gamma^e n_{cr} < 1$) in spite of the reduced heating associated with CP. The onset of relativistic transparency has been observed experimentally for the Trident Laser and nm-thick targets (< 100 nm) regardless of laser polarization [29] (where the relativistic transparency sets in early in the rise phase of the pulse). Hence, while the laser-plasma interaction is likely to include a brief RPA phase, the onset of relativistic transparency will quickly terminate the RPA phase. With LP, ion acceleration appears to be dominated by the Break-Out Afterburner (BOA) [22,28,30,31] within the relativistic transparency of the target accelerating ions to a Maxwellian energy distribution with high-energy cutoffs exceeding 40 MeV/nucleon [32,33]; however, another mechanism appears to be occurring with CP.

In the experiments, the laser is focused by an $F/3$ off-axis parabolic mirror to a spot diameter of 6 μm delivering an on-target intensity of 2×10^{20} W/cm^2 in ~500 fs (160 TW, $\lambda = 1054$ nm) under normal incidence to a free standing diamondlike carbon (DLC) target. Targets with thicknesses from 5 to 60 nm were employed and the laser polarization was controlled via a quarter wave plate. Ion spectra were recorded using a Thomson parabola spectrometer [34] positioned 1.2 m behind the rear of the target (see Fig. 1) that was capable of clearly separating the different charge states at the measured energies of about 5 to 10 MeV/Nucleon to ensure measurement of uncorrupt ion spectra [32]. Isolated monoenergetic C^{6+} spectra were observed experimentally for very thin targets of 5 to 10 nm thickness and CP laser (in 2/3 of the shots), whereas LP light always resulted in exponentially decaying energy spectra. Figure 2(a) shows C^{6+} spectra obtained from 5 nm thin DLC foil targets with CP and LP. In the CP case, an isolated quasimonoenergetic spectrum peaked at 35 ± 5 MeV (2.9 ± 0.4 MeV/nucleon) with an energy spread of $\pm 15\%$, whereas the LP case resulted in an exponentially decaying energy spectrum [see Fig. 2(a)]. However, for these very thin targets it can be difficult to determine whether the measured spectra are truly exponential, as common in TNSA, or influenced by other phenomena [35]. The particle numbers within the monoenergetic feature and conversion efficiency of laser light into ion energy exceed those obtained with TNSA by Hegelich *et al.* [15] by an order of magnitude. The conversion efficiency of laser energy into the monoenergetic feature has been estimated to 0.06% (assuming a particle beam with a divergence half angle of 10°). In Fig. 2(b) C^{6+} spectra from shots on 10 nm foil targets and CP laser light are shown; here, the monoenergetic character of the spectra is broadened and less distinct, which agrees with the theory and simulation explained later. With further increase in target thickness, fully exponentially decaying energy spectra are obtained (not shown) regardless of laser polarization.

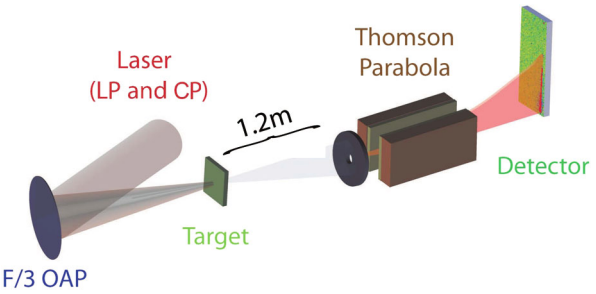

FIG. 1 (color online). Experimental setup, with the laser (CP and LP) being focused by an $F/3$ off-axis parabolic mirror on a nm-scaled diamondlike target; ions are measured with a Thomson parabola positioned 1.2 m behind the target.

To understand the experiments, ion acceleration is simulated in the transparency regime using the VPIC code. The 2D simulation domain is 20×25 μm in the (x, z) plane, where the laser propagates along x and has time-varying intensity $I(t) = I_0 \sin^2(t\pi/\tau)$ with $I_0 = 2.0 \times 10^{20}$ W/cm^2 and $\tau/2$ is the FWHM (500 fs, $\lambda = 1054$ nm). A Gaussian-shaped pulse in z is used with best focus at the target surface, where E_y, $E_z \sim \exp(-z^2/w^2)$ with $w = 6.8$ μm. The targets (C^{6+} with 5% protons in number density) are of solid density $n_e/n_{cr} = 821$ (2.8 g/cm^3) with thickness of 5 nm and a step-function profile at the beginning of the simulation. The cell size is $\Delta x = 0.3\lambda_D^0$ (0.3 nm) and $\Delta z = 1.7\lambda_D^0$ ($\lambda_D^0 = \omega_{pe}^{-1}\sqrt{T_e/m_e}$ is the initial electron Debye length); 500 electrons per cell are used ($T_e = 18$ keV and $T_i = 10$ eV for C^{6+} and protons). Absorbing boundary conditions are employed for particles and fields. In Fig. 3(a) carbon energy spectra are compared for CP (solid curves) and LP (dashed curves) laser pulses. The LP case has a broad (exponential) spectrum, whereas the CP case yields a quasimonoenergetic peak at 50 MeV, slightly higher than observed in the experiment. In the

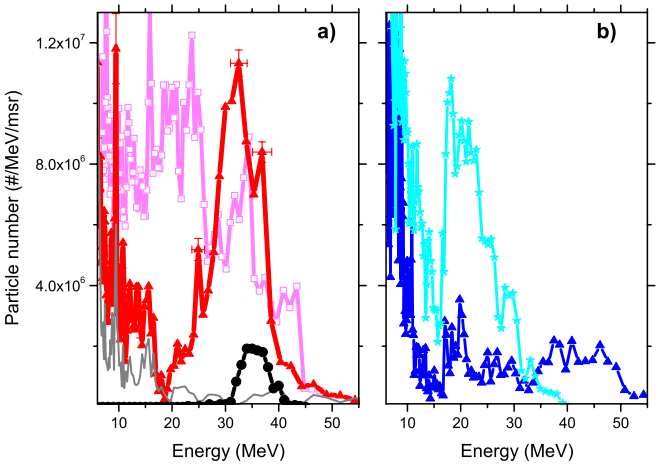

FIG. 2 (color online). (a) C^{6+} spectra measured with CP (red triangles, noise in gray) and LP (magenta squares) from a 5 nm DLC target and the C^{6+} spectrum obtained from 20 μm Pd, published in Hegelich *et al.* [15]; (b) C^{6+} spectra measured with CP from two different shots on 10 nm DLC showing deterioration of the monoenergetic structure at increased target thickness.

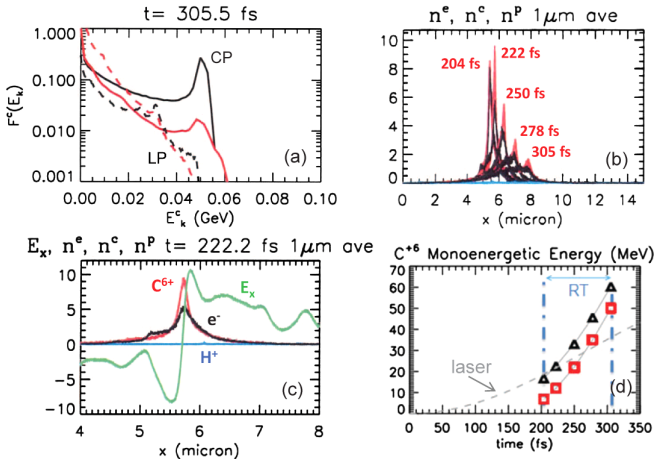

FIG. 3 (color online). Results from a 2D simulation: (a) C^{6+} spectra at 305 fs (end of the acceleration phase) for CP (solid) and LP (dashed) laser obtained along a 1-μm average over z centered at $z = 0$ (black) and from the whole simulation domain (red); (b) time evolution of carbon ion (red curves) and electron density (black), both normalized to n_{cr}, during the transparency phase (the blue trace is the proton density); (c) bipolar electric field structure in E_x (green) comoving with the solitary carbon density spike (red); (d) monoenergetic ion energy (red squares) obtained from ion spectrum vs time during the acceleration phase as compared with the soliton energy $\frac{1}{2}m_i v_p^2$ (black triangles) estimated from the soliton speed v_p (the laser intensity profile is indicated in arb. u. as gray dashed line).

simulations, the energy spread is $\pm 10\%$ which agrees well with the $\pm 15\%$ energy spread in spectra measured 120 cm behind the target (while in transit, these C^{6+} beams would expand from self-Coulomb forces not modeled in the simulation). A conversion efficiency of 0.35% of the laser energy into carbon ions of all energies, with 0.11% of the laser energy into ions with energy exceeding 40 MeV has been measured. Detailed analysis of the CP case reveals ion-acceleration based on the generation of a carbon ion soliton before and its stable propagation during the relativistic transparency of the target. It should be noted here, that the simulations of this paper were run at conditions designed to match (as close as possible) the actual experiment, which did result in weaker solitons than other conditions we have modeled (see Ref. [36]). This mechanism has two distinct stages. The first is a transient RPA phase, where the ponderomotive force of the CP laser compresses the target (a process similar to that described in previous studies of the RPA mechanism [19,37]) and a pronounced carbon ion density spike forms, as shown in Fig. 3(b) at 204 fs. During this first stage, the target distorts and the laser heats the electrons at the front surface of the target. This stage ends at $t = 204$ fs when the target turns relativistically transparent $[n_e/(\gamma^e n_{cr}) \sim 1]$. Prior to transparency, the ion energy gain is modest, about $\sim$6 MeV. After transparency, dramatic ion acceleration occurs, as shown by the squares in Fig. 3(d) where monoenergetic ion energy vs time after transparency is displayed. Associated with transparency is a persistent, sharp ion density structure that propagates and accelerates forward in x as shown in Fig. 3(b). A bipolar electric field structure in E_x, shown in Fig. 3(c) (green curve) comoves with the carbon density spike (red); the electrons, by virtue of their orbits in the intense laser field, are insufficiently mobile in x to short out E_x and their charge (black curve) and current densities vary smoothly across the soliton. Dramatic ion energy is gained starting from the onset of transparency at 204 fs and continuing to 305 fs, when the ion soliton reaches the back of the expanding target layer. The presence of ion solitons coincides with the dominant epoch of ion acceleration in the simulations. However, we do not rule out at this time that simultaneous, nonoptimized RPA-like dynamics may, in fact, also be present, but not as the dominant contributor to the acceleration. In our simulations, the most dramatic period of acceleration takes place after the onset of transparency, not before; RPA dynamics would predict a decrease in efficiency at the point of transparency. This points to an ion acceleration different from RPA being dominant. In addition, protons are here not affected by this acceleration mechanism, as they are mostly evacuated from the target by the time the acceleration phase starts due to the very low atomic content of protons in the target (about 5%) and their high charge to mass ratio, i.e., their fast response to electric fields. In fact, the measured proton energies are about an order of magnitude higher (20 MeV to 40 MeV, not shown here) than the carbon energies per nucleon. This is in contrast to an RPA-dominated acceleration and to the mechanism proposed by Qiao *et al.* [23], where the carbon ions suffer from rapid Coulomb explosion induced by the protons that are "snowplowed" ahead.

The nonlinear structures observed in the simulation appear to be ion solitons whose properties can be obtained from a generalization of the Akhiezer-Polovin (AK) problem [38,39] describing the nonlinear propagation of an intense electromagnetic wave in cold plasma. We have extended the AK theory to include ion as well as electron dynamics. A derivation of the solitary wave dynamics will be presented elsewhere [36], however we highlight parts of the derivation here. From a two-fluid relativistic description of ions and electrons (neglecting pressure) and Maxwell's equations, the local charge density is found to obey $Z_i n_i - n_e = n_e[(v_{ix} - v_{ex})/(v_p - v_{ix})]$, where n is density (subscripts i and e indicate ion and electron quantities, respectively), Z_i is ion core charge, v_x is longitudinal speed, and v_p is the speed of the soliton. A stable, localized ion density spike, as seen in Fig. 3(b), requires the ion speed across the soliton to be slightly less than the soliton speed, as seen in VPIC simulations in Fig. 3(d), where monoenergetic ion energy obtained from ion spectrum is compared to the soliton "energy" $\frac{1}{2}m_i v_p^2$. For propagation of solitons, an intense laser field must be present across the

soliton. Without such a field, the electrons short out the strong E_x associated with the soliton and prevent propagation; this is verified in our simulations at times before burn-through (not shown here), when a density spike forms, but does not propagate. In this regard, our solitons are fundamentally different from, e.g., laser-driven ion-acoustic solitons considered previously [35]. The free energy accelerating particles in the soliton comes from the laser field during the transparency phase. The soliton ion density spike gives rise to a longitudinal electric field, which changes the electron parallel momentum p_x across the soliton. The relatively slowly varying change in p_x leads to a corresponding change in laser index of refraction in the vicinity of the soliton. This variation reflects some of the laser light from the soliton, leading to an enhancement of the electrostatic field further accelerating the ions and sharpening the ion density spike. The rate of energy coupling within the soliton can be increased by having a larger initial ion density spike (i.e., larger variation in electron γ across the soliton and thus larger change in index of refraction) or by having a larger laser amplitude, so that the rate of laser light momentum transfer into the soliton is larger. Additional simulations [36] show that the laser field at $I_0 = 2 \times 10^{20}$ W/cm^2 is not sufficiently intense to generate the necessary density spike in the ion distribution and hence cannot generate a sharp monoenergetic ion beam; indeed, the experimental spectra for the 10 nm target cases in Fig. 2(b) show deteriorated monoenergetic ion features. In conclusion, in this experiment we observe for the first time laser-driven monoenergetic ions from nanotargets in conjunction with circularly polarized laser pulses. We presented high-resolution 2D-VPIC simulations consistent with the measured data. In these simulations the formation of an ion soliton during the relativistic transparency of the target appears to be responsible for accelerating these beams. This regime, experimentally accessible with current lasers, marks a step toward to realization of laser-ion-acceleration based applications. Energies obtained here are sufficient to interact with tumors situated on or near the human skin. They also mark progress towards future developments of laser-plasma particle accelerators, such as ion injectors, inertial confinement fusion, proton radiography and oncology that require high-flux monoenergetic ion beams. Further increase of the laser intensity and optimization of the temporal and spatial pulse profile as well as the target promises to open up new exciting possibilities of laser-driven ion acceleration in many fields across fundamental as well as applied sciences.

We are grateful for the support of the Trident laser team and J. Szerypo and P. Hilz from the LMU target group. The VPIC simulations were run on the LANL Roadrunner supercomputer. Work was supported by: DOE OFES, Deutsche Forschungsgemeinschaft (DFG) Transregio SFB TR18, Cluster of Excellence (MAP) and LMU-Excellence (M. Hegelich).

*daniel.jung@physik.uni-muenchen.de

[1] G. A. Mourou, T. Tajima, and S. V. Bulanov, Rev. Mod. Phys. **78**, 309 (2006).
[2] R. A. Snavely *et al.*, Phys. Rev. Lett. **85**, 2945 (2000).
[3] M. Hegelich *et al.*, Phys. Rev. Lett. **89**, 085002 (2002).
[4] B. M. Hegelich *et al.*, Phys. Plasmas **12**, 056314 (2005).
[5] J. Schreiber *et al.*, Appl. Phys. B **79**, 1041 (2004).
[6] T. E. Cowan *et al.*, Phys. Rev. Lett. **92**, 204801 (2004).
[7] F. Pegoraro *et al.*, Laser Part. Beams **22**, 19 (2004).
[8] M. Borghesi *et al.*, Plasma Phys. Controlled Fusion **43**, A267 (2001).
[9] J. C. Fernández *et al.*, J. Phys. Conf. Ser. **112**, 022051 (2008).
[10] J. J. Honrubia *et al.*, J. Phys. Conf. Ser. **244**, 022038 (2010).
[11] S. P. Hatchett *et al.*, Phys. Plasmas **7**, 2076 (2000).
[12] J. Fuchs *et al.*, Nature Phys. **2**, 48 (2005).
[13] A. P. L. Robinson, A. R. Bell, and R. J. Kingham, Phys. Rev. Lett. **96**, 035005 (2006).
[14] S. A. Gaillard *et al.*, Phys. Plasmas **18**, 056710 (2011).
[15] B. M. Hegelich *et al.*, Nature (London) **439**, 441 (2006).
[16] H. Schwoerer *et al.*, Nature (London) **439**, 445 (2006).
[17] O. Klimo *et al.*, Phys. Rev. ST Accel. Beams **11**, 031301 (2008).
[18] A. P. L. Robinson *et al.*, Plasma Phys. Controlled Fusion **51**, 024004 (2009).
[19] X. Q. Yan *et al.*, Phys. Rev. Lett. **100**, 135003 (2008).
[20] A. Macchi, S. Veghini, and F. Pegoraro, Phys. Rev. Lett. **103**, 085003 (2009).
[21] T. Esirkepov *et al.*, Phys. Rev. Lett. **92**, 175003 (2004).
[22] L. Yin *et al.*, Phys. Plasmas **14**, 056706 (2007).
[23] B. Qiao *et al.*, Phys. Rev. Lett. **105**, 155002 (2010).
[24] A. Henig *et al.*, Phys. Rev. Lett. **103**, 245003 (2009).
[25] K. J. Bowers *et al.*, Phys. Plasmas **15**, 055703 (2008).
[26] J. Workman *et al.*, Rev. Sci. Instrum. **79**, 10E905 (2008).
[27] R. C. Shah *et al.*, Opt. Lett. **34**, 2273 (2009).
[28] A. Henig *et al.*, Phys. Rev. Lett. **103**, 045002 (2009).
[29] R. Shah *et al.*, Nature Phys. (to be published).
[30] B. J. Albright *et al.*, Phys. Plasmas **14**, 094502 (2007).
[31] S. Steinke *et al.*, in *Quantum Electronics and Laser Science Conference* (Optical Society of America, 2010), p. JFB1.
[32] D. Jung *et al.*, Rev. Sci. Instrum. **82**, 013306 (2011).
[33] B. M. Hegelich *et al.*, Nucl. Fusion **51**, 083011 (2011).
[34] J. J. Thomson, Philos. Mag. Series 6, **22**, 469 (1911).
[35] A. Zhidkov *et al.*, Phys. Rev. Lett. **89**, 215002 (2002).
[36] L. Yin *et al.*, Phys. Plasmas **18**, 053103 (2011).
[37] A. P. L. Robinson *et al.*, New J. Phys. **10**, 013021 (2008).
[38] A. I. Akhiezer and R. V. Polovin, Sov. Phys. JETP **3**, 696 (1956).
[39] R. J. Noble, Phys. Rev. A **32**, 460 (1985).